PAPER

Check for updates

Sensitive and rapid DPV detection of urinary homovanillic acid *via* g-C₃N₄@nZVI modified carbon paste sensor

Aya A. Mouhamed, [iD] *[a] Maria Osama Mekhail, [iD] [b] Tony Victor Zaki, [iD] [b] Amr M. Mahmoud [iD] [a] and Aya T. Soudi [iD] [a]

Non-invasive and rapid detection of HVA, a validated urinary biomarker for neuroblastoma and catecholamine-secreting cancers, remains analytically challenging due to its low physiological levels and interference from common urinary components. Herein, a novel electrochemical sensing platform is introduced by integrating a graphitic carbon nitride (g-C₃N₄) and nanoscale zero-valent iron (nZVI) composite into a carbon paste electrode (CPE) and employing differential pulse voltammetry (DPV) for HVA quantification in urine. The g-C₃N₄@nZVI composite synergistically enhances electron transfer kinetics and suppresses non-faradaic background current, leading to lower baseline noise and superior signal resolution. Under optimized voltammetric conditions, the sensor exhibits a broad linear response from 2 μM to 100 μM, with a detection limit of 0.978 μM that encompasses physiological urinary HVA levels (8–41 μM). Structural characterization *via* SEM/EDX confirmed uniform deposition of iron nanoparticles on the g-C₃N₄ matrix, and electrochemical tests revealed diffusion-controlled, irreversible oxidation of HVA. Analysis of spiked human urine yielded recoveries within 95–98% and intra-day/inter-day precision with RSD < 2%, confirming the method's accuracy and reproducibility. Compared to existing voltammetric platforms, this sensor achieves enhanced selectivity, operates at near-neutral pH without complex buffering, and supports portable deployment. Overall, the g-C₃N₄@nZVI/CPE with DPV offers a sensitive, fast, and cost-effective tool for point-of-care HVA screening in clinical settings.

1. Introduction

Early detection of cancer through non-invasive biomarker assays has been a long-standing goal in oncology, aiming to improve patient prognosis by identifying the disease at its earliest, most treatable stages.[1] Among urinary metabolites, homovanillic acid (HVA), the primary oxidative breakdown product of dopamine, has been clinically validated as a biomarker for neuroblastoma and other catecholamine-secreting malignancies. Elevated HVA levels correlate strongly with tumor burden and can aid prognosis estimation in localized disease.[2–4] However, detecting HVA in urine remains challenging due to its low physiological concentrations and interference from complex urinary matrices, such as urea and creatinine, which hinder accurate quantification.[5]

Traditional analytical techniques for quantifying HVA include high-performance liquid chromatography (HPLC),[6–19] liquid chromatography coupled with mass spectrometry (HPLC-MS/MS),[20–22] and gas chromatography with a mass detector,[23] all

of which offer high specificity and low detection limits but require preliminary sample preparation, expensive equipment, and skilled personnel. Immunoassays such as ELISA which depends on labeled antibodies, involve multi-hour incubations, and often lack the throughput and portability required for point-of-care testing (POCT).[24] One amperometry method[25] was reported that requires strongly acidic conditions (pH 3.0) to resolve and detect HVA peaks, necessitating sample pretreatment that may complicate direct urine analysis. In addition to the use of costly boron-doped diamond electrodes without on-line sample clean-up limits sensitivity and specificity in complex biological fluids. Electrochemical sensing has emerged as a rapid, cost-effective, and portable alternative for HVA detection. However, most existing platforms[2,26–28] lack the sensitivity and selectivity for clinical applications and require strongly acidic conditions, necessitating external buffering of urine samples. To address these gaps, this work introduces a novel composite material, graphitic carbon nitride (g-C₃N₄) loaded with nanoscale zero-valent iron (nZVI), integrated into a carbon paste electrode (CPE).

Graphitic carbon nitride (g-C₃N₄) has emerged as a versatile, metal-free semiconductor with a high specific surface area, tunable electronic band structure, and exceptional chemical stability under physiological conditions,[29] enabling its use in

[a]Department of Pharmaceutical Analytical Chemistry, Faculty of Pharmacy, Cairo University, Kasr El-Aini Street, ET-11562, Cairo, Egypt. E-mail: aya.soudi@pharma.cu.edu.eg

[b]Faculty of Pharmacy, Cairo University, Kasr El-Aini Street, ET-11562, Cairo, Egypt

diverse biomedical and analytical applications, including stimuli-responsive delivery systems and diagnostic platforms.[30–32] Its nitrogen-rich architecture facilitates facile functionalization and serves as an excellent scaffold for heteroatom doping and nanoparticle embedding, broadening its applications in photocatalysis, energy conversion, and sensing.[33,34]

Nanoscale zero-valent iron (nZVI) particles exhibit strong redox activity and rapid electron-transfer kinetics, making them effective for use in environmental remediation and electrochemical systems.[35,36] However, unsupported nZVI tends to agglomerate and oxidize, reducing active surface area.[36] Anchoring nZVI onto the porous matrix of g-C_3N_4 not only stabilizes the iron cores against passivation but also creates a synergistic interface in which the high conductivity and catalytic sites of nZVI complement the large surface area and structural robustness of g-C_3N_4.[37]

Carbon paste electrodes (CPEs) comprised of graphite powder mixed with a binder like mineral oil are especially well-suited for point-of-care electrochemical diagnostics due to their low background current, wide potential window, and easily renewable surfaces, along with their simplicity and low cost in fabrication.[38,39] They support on-site, disposable use without complex cleaning, allowing easy incorporation of nanocomposites directly into the paste for reagent-free sensors with tailored surface chemistry.[38,40] These properties facilitate integration with portable potentiostats, enabling miniaturized, low-cost, and user-friendly POC platforms.

Differential Pulse Voltammetry (DPV) applies incremental potential with small, repeated pulses superimposed on a linear sweep. By sampling current just before and at the end of each pulse and plotting their difference *versus* potential, DPV suppresses the charging (non-faradaic) current, isolating the faradaic signal.[41,42] This results in sharp, well-defined peaks where the height is directly proportional to analyte concentration.[41,43,44] Moreover, DPV offers significantly higher sensitivity alongside better resolution between closely spaced redox events and minimal sample volume requirements, making it particularly suited for portable, battery-powered analyzers.[42]

The drive toward decentralized diagnostics has spurred development of lab-on-a-chip systems and portable electrochemical devices,[45–48] specially for cancer biomarker detection.[49] Miniaturized DPV platforms, when combined with composite-modified CPEs, have the potential to deliver rapid, on-site HVA screening directly from urine samples, bypassing the need for centralized laboratories and significantly reducing the assay time. Additionally, using urine offers a non-invasive and easily accessible means of screening, improving patient comfort and compliance.[50,51]

Comprehensive physicochemical characterization of g-C_3N_4@nZVI composites typically employs scanning electron microscopy (SEM) to assess morphology and confirms the uniform distribution and size of the embedded nZVI nanoparticles.[52,53] Complementing this, Energy-Dispersive X-ray Spectroscopy (EDX) mapping confirmed the elemental composition and homogeneous dispersion of iron within the g-C_3N_4 matrix.[54] This streamlined characterization confirms successful composite synthesis and highlights its structural integrity without unnecessary additional techniques.

To our knowledge, no previous research has integrated a g-C_3N_4@nZVI hybrid into a CPE for the rapid and direct electrochemical detection of HVA in urine. We thus introduce such platform, combining the catalytic advantages of g-C_3N_4@nZVI with the simplicity of a CPE and the precision of DPV. This novel approach offers improved sensitivity, fast response times, high selectivity against common urinary interferences, and robust performance in real-sample matrices. This point-of-care sensor platform promises a cost-effective, user-friendly tool for early cancer biomarker screening and monitoring.

2. Experimental

2.1. Materials and reagents

Homovanillic acid (99%), melamine, ferric chloride (FeCl$_3$), sodium borohydride (NaBH$_4$), sodium hydroxide (NaOH), graphite, and phosphate-buffered saline (PBS) tablets were procured from Sigma-Aldrich (Germany). Paraffin oil, used as the binder in carbon paste preparation, was supplied by Merck KGaA (Darmstadt, Germany). HPLC-grade ethanol was obtained from Fisher Scientific (Loughborough, UK), and deionized water (double-distilled) was produced on-site using an Agela Technologies system (Wilmington, USA).

2.2. Instrumentation

A Corrtest CS100 portable potentiostat/galvanostat (Wuhan, China) was employed for electrochemical measurements in a three-electrode configuration: an Ag/AgCl reference electrode, a platinum wire serving as the counter electrode, and the g-C_3N_4@nZVI carbon paste electrode functioning as the working electrode. This lightweight device is suitable for portable applications including DPV measurements. Solution pH was adjusted using a Jenway 3330 digital ion analyser with a glass pH electrode (Jenway, Essex, UK) to ensure precise pH adjustment of test solutions. Morphological analysis of the g-C_3N_4@nZVI composite was conducted using a ZEISS EVO scanning electron microscope.

2.3. Procedure

2.3.1. Standard solution preparation. A stock HVA solution was prepared by dissolving 45.5 mg of HVA in a 25 mL volumetric flask with deionized water, then filling to the mark. From this, 1 mL was pipetted into a second 25 mL flask and diluted to the mark, resulting in a 1×10^{-3} M HVA solution.

2.3.2. Fabrication of g-C_3N_4@nZVI composite. Graphitic carbon nitride (g-C_3N_4) was synthesized by heating melamine in an oven at 550 °C for 4 hours, followed by annealing at 500 °C for an additional 2 hours.[55] The resulting yellowish powder was washed, dried, and ground to obtain g-C_3N_4. A total of 200 mg of g-C_3N_4 powder was dispersed in 20.0 mL of distilled water and subjected to ultrasonication for 10 minutes to achieve uniform dispersion. Subsequently, an aqueous solution of FeCl$_3$, 4 mg mL^{-1} was added and manually stirred with a glass rod for 15.0 minutes. To initiate the reduction reaction, 1.0 mL of NaBH$_4$

solution was added dropwise over 10 minutes under continuous magnetic stirring at 300 rpm. The reaction followed a liquid-phase reduction pathway, resulting in the formation of zero-valent iron nanoparticles (nZVI), which appeared as a black suspension. To ensure complete reduction, the reaction mixture was stirred for an additional 10.0 minutes. The resulting g-C_3N_4@nZVI composite was collected by centrifugation, thoroughly washed three times by water and last time by ethanol and dried in an oven at 60 °C for 30 minutes to yield the final purified product. Fig. S1 visually encapsulates each stage: thermal treatment, dispersion, iron loading, reduction, washing, and drying, providing a clear and concise overview of the synthesis protocol.

2.3.3. Fabrication of g-C_3N_4@nZVI modified carbon paste electrodes. CPEs containing varying percentages of the synthesized g-C_3N_4@nZVI composite were prepared as follows: specific amounts of graphite powder were weighed and placed into a mortar. Subsequently, different amounts of the g-C_3N_4@nZVI composite (1.0, 2.0, 5.0, and 10.0 mg) were added, corresponding to 1%, 2%, 5%, and 10% (w/w) relative to the total paste composition (200.0 mg). The mixtures were thoroughly homogenized with 0.50 mL of paraffin oil for at least 5 minutes to ensure uniform dispersion. The resulting modified electrodes were designated as 1% g-C_3N_4@nZVI/CPE, 2% g-C_3N_4@nZVI/CPE, 5% g-C_3N_4@nZVI/CPE, and 10% g-C_3N_4@nZVI/CPE, respectively. Each modified paste was filled in the electrode body and a copper wire was used for electrode connection. The plain CPE was prepared in the same procedure without g-C_3N_4@nZVI mixing. The new surface of the paste electrode surface was simply renewed by scraping off about 3.0 mm of its old surface and polishing the new surface with a piece of tracing paper.

2.3.4. Operational conditions of electrochemical measurements. Voltammetric measurements were performed at room temperature using cyclic voltammetry (CV) and DPV to investigate the electrochemical behavior of HVA. A detailed CV analysis, by sweeping the potential from -0.10 to $+1.20$ V, was conducted in an electrolyte solution containing 1.0 mM potassium ferricyanide $[K_3[Fe(CN)_6]]$ for characterizing the electrochemical properties of g-C_3N_4@nZVI/CPE and bare CPE. The voltammetric response of HVA was examined at g-C_3N_4@nZVI/CPE by recording voltammograms at different scan rates (10 to 200 mV s^{-1}). For quantification, DPV was carried out under controlled conditions including a pulse amplitude set to 0.07 V, pulse width (modulation time) to 0.095 s, and pulse period (interval) to 0.5 s. DPV voltammograms in the anodic region, ranging from -0.20 V to $+1.2$ V, were carefully studied. These techniques together with optimized parameters provided a clear and detailed study of the electrochemical properties of HVA.

2.3.5. Construction of calibration curve. Aliquots of HVA were transferred from its stock solution into different 25 mL volumetric flasks. The volume was then precisely adjusted to achieve final concentrations ranging from 2 μM to 100 μM using PBS solution at pH 7.0. DPV was performed within a potential range from -0.20 V to $+1.2$ V. The peak current recorded for each sample was plotted against its respective concentration to construct the calibration curve and determine the regression equation.

2.3.6. Method validation. The developed method was successfully validated following ICH guidelines[56] for linearity, accuracy, precision, detection, and quantification limits, confirming its suitability for the intended use. Linearity was thoroughly investigated under optimal electrochemical conditions by analyzing six different concentrations of HVA. Accuracy was assessed by calculating the percentage recovery of three different concentrations. Intra-day and inter-day precision were evaluated and reported as % RSD.

2.3.7. Analysis of HVA in urine. To analyze urine samples, 1.0 mL of urine was spiked with precise amounts of HVA stock solution and the mixture was then diluted to a final volume using phosphate buffer pH 6 to achieve the desired concentration. Adjustment of the pH was performed to ensure consistency and optimize the analytical conditions for our voltammetric method to determine HVA with accuracy and reproducibility in the prepared urine samples.

3. Results and discussion

The g-C_3N_4@nZVI-modified carbon paste electrode (CPE) demonstrated strong electrochemical performance: DPV produced sharp, concentration-dependent peaks, with enhanced sensitivity and well-defined responses. SEM combined with EDX confirmed a uniform distribution of nZVI nanoparticles throughout the g-C_3N_4 matrix, which enhances electron transfer and resists fouling. Integrating this nanocomposite CPE with DPV represents a novel, rapid, and portable solution for direct HVA screening, advancing point-of-care cancer biomarker detection.

3.1. Surface characterization of g-C_3N_4@nZVI-modified carbon paste electrode

Surface characterization of the g-C_3N_4@nZVI composite was performed using scanning electron microscopy (SEM) in combination with energy-dispersive X-ray spectroscopy (EDX). As shown in Fig. 1, the SEM micrograph reveals a rough, aggregated surface composed of crumpled and stacked lamellar domains, which are characteristic of graphitic carbon nitride. The layered framework is decorated with numerous fine granular features distributed over the surface, giving rise to a heterogeneous yet compact morphology. These nanoscale domains are attributed to the incorporation of nZVI within the g-C_3N_4 matrix. Importantly, no large or isolated iron-rich agglomerates are observed, indicating effective dispersion of iron species throughout the composite. The elemental composition and spatial distribution were further evaluated by EDX analysis and elemental mapping (Fig. 2). The EDX spectrum confirms the presence of carbon, nitrogen, oxygen, and iron, consistent with the expected composition of the g-C_3N_4@nZVI composite. Elemental mapping images demonstrate a homogeneous distribution of carbon and nitrogen across the layered framework, while iron signals are uniformly dispersed throughout the same regions, corroborating the successful
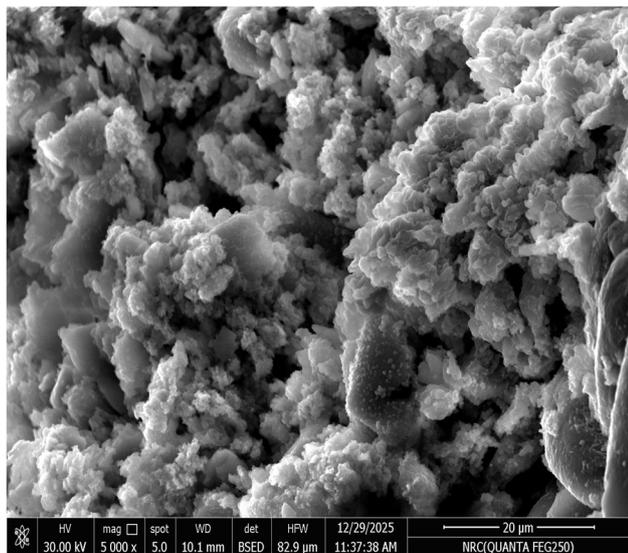
Fig. 1 SEM image of g-C$_3$N$_4$@nZVI shows a rough, aggregated surface composed of crumpled and stacked lamellar domains, which are characteristic of graphitic carbon nitride. The layered framework is decorated with numerous fine granular features distributed over the surface, giving rise to a heterogeneous yet compact morphology.

immobilization of nZVI within the g-C$_3$N$_4$ structure. The detected oxygen is attributed to surface oxidation and oxygen-containing functional groups associated with both g-C$_3$N$_4$ and iron species.

The FTIR spectrum of the g-C$_3$N$_4$@nZVI nanocomposite (Fig. S2) confirms the preservation of the graphitic carbon nitride framework after iron incorporation. The broad absorption band in the 3000–3400 cm^{-1} region is attributed to –NH and –OH stretching vibrations from residual amino groups and surface-adsorbed moisture. The strong bands observed between 1200 and 1650 cm^{-1} correspond to characteristic C–N and C=N stretching modes of the tri-s-triazine units, while the band near ~800 cm^{-1} is assigned to the breathing mode of the s-triazine ring, a fingerprint feature of g-C$_3$N$_4$.

Following the incorporation of nZVI, no distinct bands related to crystalline iron oxides are detected, indicating that the iron species are highly dispersed within the g-C$_3$N$_4$ matrix. Subtle changes in band intensity suggest interfacial interactions between g-C$_3$N$_4$ and nZVI, supporting successful composite formation without disruption of the host structure. This retained framework is advantageous for efficient charge transport during electrochemical sensing.

X-ray diffraction was employed to examine the crystalline features of the g-C$_3$N$_4$@nZVI nanocomposite (Fig. S3). The diffractogram displays a dominant reflection at around 27.4°, which is characteristic of the (002) interlayer stacking of graphitic carbon nitride, confirming the preservation of its layered structure after composite formation. A weak and broad feature near 13° can be attributed to the in-plane structural packing of the tri-s-triazine units of g-C$_3$N$_4$. No distinct diffraction peaks attributable to crystalline iron or iron oxides are observed in the XRD pattern. This is likely due to the low loading level, nanoscale dimensions, and high dispersion of nZVI particles within the g-C$_3$N$_4$ matrix, which can render iron phases XRD-amorphous. As a result, while XRD confirms the structural integrity of g-C$_3$N$_4$, it cannot unambiguously distinguish between Fe^0 and oxidized iron species in the composite. Therefore, the presence and uniform incorporation of iron are further supported by SEM–EDX mapping and the pronounced enhancement in electrochemical performance, which is consistent with reports on nZVI-based composites in the literature.
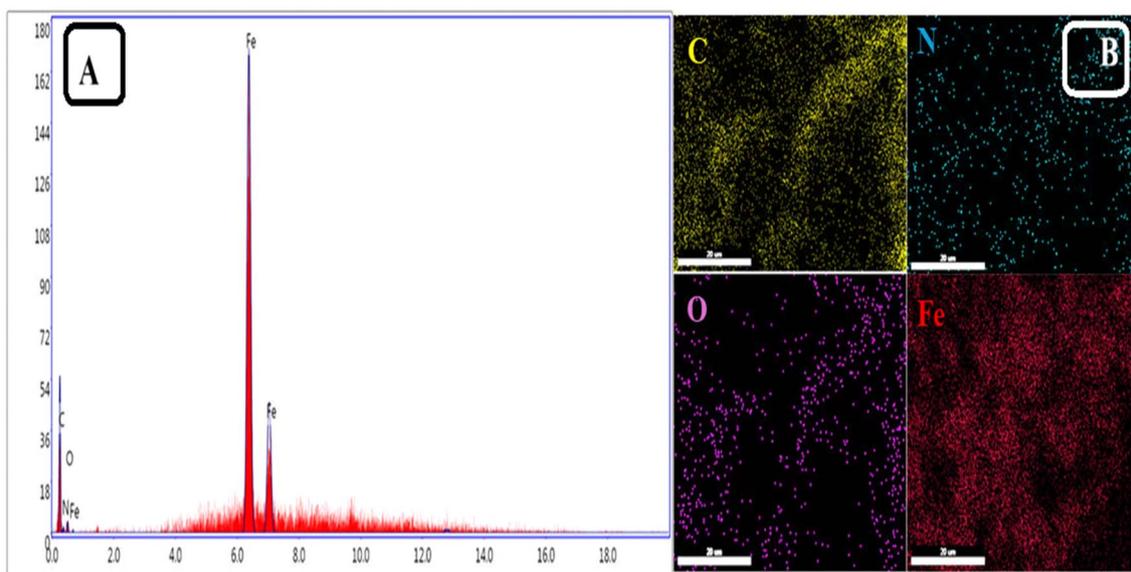

Fig. 2 (A) EDX spectrum of g-C$_3$N$_4$@nZVI confirm the presence of carbon (C), nitrogen (N), oxygen (O), and iron (Fe) and (B) EDS elemental mapping images of g-C$_3$N$_4$@nZVI show the distribution of carbon (C), nitrogen (N), oxygen (O), and iron (Fe).

Nitrogen adsorption–desorption measurements were performed to evaluate the textural properties of the g-C$_3$N$_4$@nZVI nanocomposite. As shown in Fig. S4, the material exhibits a type-IV isotherm with a pronounced uptake at higher relative pressures ($P/P_0 > 0.8$), indicative of a mesoporous structure. The corresponding BET plot shows good linearity within the appropriate pressure range, confirming the validity of the surface area analysis. The specific surface area calculated using the Brunauer–Emmett–Teller (BET) method was 11.826 m^2 g^{-1}, supporting the claim that the g-C$_3$N$_4$ framework provides a high-surface-area matrix for nanoparticle immobilization. The presence of mesopores and accessible surface sites is expected to facilitate analyte diffusion and enhance electroactive site availability, contributing to the improved electrochemical response observed for HVA sensing.

Together, these structural, compositional, and textural analyses confirm the successful fabrication of a well-integrated g-C$_3$N$_4$@nZVI nanocomposite with uniform iron dispersion and accessible surface area, providing a solid structural basis for the enhanced electrochemical activity observed during HVA detection.

3.2. Electrochemical characterization of g-C$_3$N$_4$@nZVI-modified carbon paste electrode

The electrochemical potential window, which defines the range of voltages an electrode can effectively operate within, is a key factor influencing its practical applications. To compare the performance of the modified and unmodified electrodes, cyclic wave voltammograms were recorded under identical conditions, and are presented in Fig. S5. The modified g-C$_3$N$_4$@nZVI/CPE electrode displayed a larger response, than the unmodified one. Furthermore, differential pulse voltammograms of the Fe^{2+}/Fe^{3+} redox system were recorded at the nZVI/CPE, g-C$_3$N$_4$/CPE, and g-C$_3$N$_4$@nZVI/CPE electrodes. Among these, the g-C$_3$N$_4$@nZVI-modified electrode displayed a substantially higher cathodic peak current along with sharper peak features relative to the electrodes containing the individual components. This enhancement can be attributed to the synergistic interaction between g-C$_3$N$_4$ matrix and nZVI particles, resulting in improved electrochemical performance (Fig. S6).

In addition, the electroactive surface area (ECSA) of the electrodes was estimated using the Fe^{2+}/Fe^{3+} redox probe. The g-C$_3$N$_4$@nZVI/CPE exhibited a markedly larger ECSA (0.18 cm^2) compared to the bare CPE (0.09 cm^2), confirming that incorporation of the nanocomposite significantly increases the number of accessible electroactive sites. This enlarged surface area facilitates enhanced charge transfer and contributes directly to the observed increase in peak current response.

The layered g-C$_3$N$_4$ structure provides a high surface area and conductive network,[29] while the uniformly distributed zero-valent iron nanoparticles facilitate rapid electron transfer and improved catalytic activity.[35,36] This leads to a more efficient oxidation of HVA, evidenced by the increased peak current and better peak definition. Importantly, the inclusion of the g-C$_3$N$_4$@nZVI nanocomposite within the carbon paste significantly suppresses the capacitive (non-faradaic) current at the

electrode interface. This led to a lower and cleaner baseline current, which directly enhances the detectable faradaic signal margin. As non-faradaic currents are greatly reduced, even low-level analyte oxidation produces sharper and more distinguishable peaks. Consequently, this leads to improved sensitivity and a lowered detection limit. Collectively, these observations confirm that the g-C$_3$N$_4$@nZVI composite significantly enhances the electrochemical sensing capabilities of the CPE, making it well suited for point-of-care HVA detection.

3.3. Electrochemical impedance spectrometry (EIS) measurements

EIS was carried out using the $[Fe(CN)_6]^{3-}/[Fe(CN)_6]^{4-}$ redox system to investigate the interfacial electron-transfer characteristics of the electrodes. The charge-transfer resistance (R_{ct}) value was reduced from 279 Ω for the bare CPE to 164 Ω for the g-C$_3$N$_4$@nZVI/CPE, confirming the successful immobilization of the nanocomposite on the electrode surface. The improved conductivity of the g-C$_3$N$_4$@nZVI nanostructure facilitated faster electron transfer, thereby enhancing the electrochemical performance of the modified electrode.

3.4. Voltammetric method optimization

3.4.1. Different percentage of the g-C$_3$N$_4$@nZVI composite.
The electrochemical performance of g-C$_3$N$_4$@nZVI-modified CPE with varying percentages of added g-C$_3$N$_4$@nZVI composite (1%, 2%, 5%, and 10%) was investigated and compared. Among these, the 2% g-C$_3$N$_4$@nZVI-modified CPE demonstrated the highest electrochemical activity, yielding a higher current response as shown in Fig. 3.

3.4.2. Optimization of DPV conditions.
The optimization of key DPV parameters such as pulse amplitude, pulse width, and pulse period was undertaken to maximize the analytical performance of the g-C$_3$N$_4$@nZVI-modified CPE for HVA detection. Pulse amplitude was varied between 0.05–0.07 V. At 0.05 V, the oxidation peak was relatively modest; increasing to 0.07 V enhanced current response and peak definition. Thus, 0.07 V was selected as the optimal amplitude, balancing
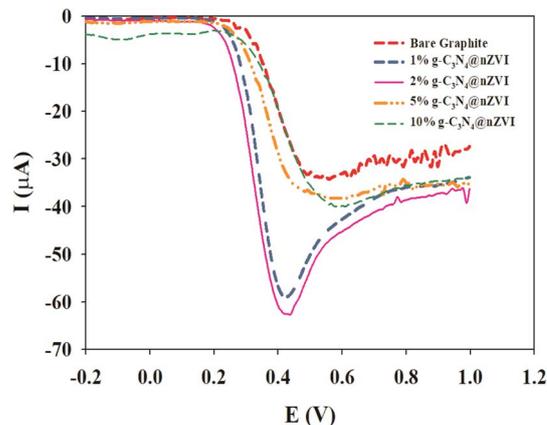

Fig. 3 DPV of CPE with different percentage of g-C$_3$N$_4$@nZVI in 1.0 mM HVA using PBS pH 6.

sensitivity against signal clarity (Fig. S7A). Pulse width (modulation time) was then adjusted (0.095–0.105 s). A width of 0.095 s provided the most intense and well-defined peak (Fig. S7B). Pulse period (interval time) was varied between 0.5–0.7 s. A period of 0.5 s yielded a sharp, high current peak with minimal baseline drift (Fig. S7C). These findings align with established DPV theory, which notes that proper adjustment of pulse amplitude, duration, and spacing enhances the ratio of faradaic to capacitive current, sharpens peak shapes, and lowers detection limits.[57]

3.4.3. Effect of pH. The influence of solution pH on the electrochemical oxidation of HVA was examined across the pH range of 6.0 to 8.0 in PBS. As illustrated in Fig. S8, the anodic peak current varied significantly with pH, indicating that proton concentration affects the electrode reaction kinetics. At pH 6.0, the peak current reached its maximum, suggesting enhanced electron transfer under slightly acidic conditions, so pH 6.0 was chosen for subsequent measurements.

3.4.4. Effect of scan rate. The influence of scan rate on the electrochemical behavior of HVA was examined using the g-C$_3$N$_4$@nZVI-modified CPE over a range of 10 to 200 mV s^{-1}. As shown in Fig. 4, increasing the scan rate resulted in a proportional rise in the anodic peak current (I_p), accompanied by a shift in peak potential toward more positive values, indicating the irreversibility of the oxidation process.[58] A linear relationship ($R^2 = 0.9962$) was observed between I_p and the square root of the scan rate ($v^{1/2}$), as illustrated in Fig. S9, suggesting a diffusion-controlled mechanism. However, the non-zero intercept of this plot implies that additional factors, such as weak adsorption interactions, may also be contributing.[58] Additionally, a linear regression analysis between the logarithm of the scan rate ($\log v$) and the $\log I_p$ was performed, yielding a slope of 0.3757 (Fig. S10). Since the measured slope is significantly below unity, it confirms that the oxidation of HVA at the g-C$_3$N$_4$@nZVI-modified carbon paste electrode is predominantly governed by diffusion of HVA molecules from the bulk solution to the electrode surface with minimal contribution from surface adsorption.[58] These deviations can be reasonably attributed to finite diffusion and thin-layer effects associated with the porous g-C$_3$N$_4$@nZVI composite layer,
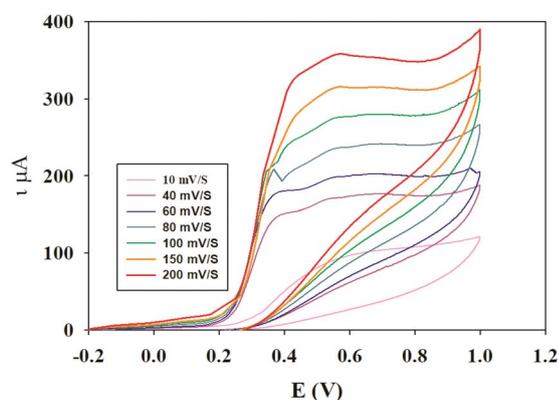
which may partially confine HVA molecules within the electrode matrix.[59] Moreover, the irreversible nature of HVA oxidation, involving a proton-coupled electron transfer followed by a rapid chemical transformation of the oxidation intermediate,[60] introduces kinetic limitations that further reduce the apparent slope.

3.5. Suggested mechanism of HVA electrochemical oxidation

HVA is a catechol derivative featuring both hydroxyl and methoxy substituents on an aromatic ring, typically undergoes an irreversible two-electron, two-proton oxidation at carbon-based electrodes, as reported in earlier studies.[60] This reaction produces a quinone-like oxidation product, consistent with the known behaviors of catechol-containing compounds undergoing proton-coupled electron transfer. In the context of the g-C$_3$N$_4$@nZVI-modified CPE, the proposed mechanism begins with adsorption of HVA onto the composite surface. The initial anodic electron transfer oxidizes the dihydroxy moiety into a corresponding quinone species, releasing two electrons and two protons (Fig. 5). Concurrently, the surface-bound iron (nZVI) in the composite facilitates electron shuttling or catalytic oxidation through an electrochemical promotion of catalysis effect, enhancing charge transfer efficiency and lowering overpotential.[35,36] During CV, the absence of a reverse cathodic peak confirms the irreversibility of HVA oxidation, indicative of further chemical transformation of the oxidation intermediate. DPV yields well-defined peaks whose heights scale with HVA concentration, supporting the dominance of this irreversible, diffusion-driven oxidation pathway.

3.6. Analytical performance of HVA on g-C$_3$N$_4$@nZVI-modified CPE

The incorporation of g-C$_3$N$_4$@nZVI into the CPE significantly enhanced its electrochemical response toward HVA. CV performed in PBS (pH 6.0) with HVA revealed a single anodic peak at approximately 0.42 V and no corresponding cathodic return peak, confirming the irreversible nature of HVA oxidation. Compared to the unmodified CPE, the modified electrode exhibited a substantially larger peak current and favorable shift in oxidation potential, indicative of improved sensitivity and catalytic activity. This enhancement enabled an extended linear dynamic range and lower detection limit in HVA quantification. Given these findings, DPV was selected for quantitative analysis due to its superior analytical qualities, particularly its ability to suppress capacitive (non-faradaic) current through pre- and post-pulse current subtraction, resulting in cleaner baselines
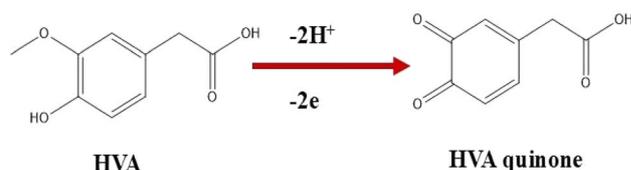

Fig. 4 Cyclic voltammograms of 1.0 mM HVA in PBS (pH = 6) on the 2% g-C$_3$N$_4$@nZVI/CPE at different scanning rates (10–200 mV s^{-1}).

Fig. 5 Suggested mechanism for HVA oxidation.

RSC Advances
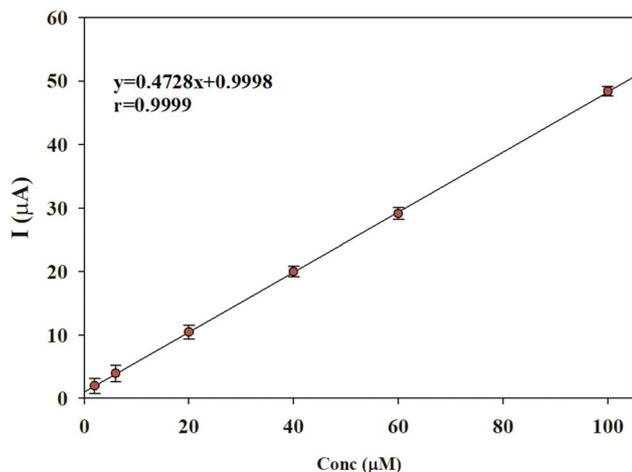
Fig. 6 The peak current plot as a function of the concentration of HVA using 2% g-C$_3$N$_4$@nZVI/CPE in PBS (pH = 6).
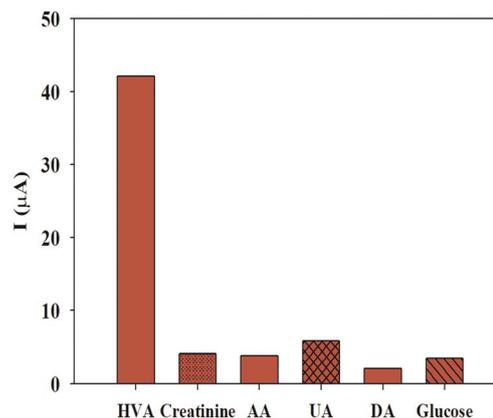

Fig. 7 DPV responses of 1.0 mM HVA and equimolar concentration of interfering substances (creatinine, ascorbic acid, uric acid, dopamine, and glucose) using phosphate buffer (PH = 6) at the surface of g-C$_3$N$_4$@nZVI/CPE.

and sharper, high-resolution oxidation peaks.[41,42] Under optimized pulse conditions (0.07 V amplitude, 0.095 s width, 0.5 s period), DPV measurements of HVA across 2–100 μM yielded highly reproducible current responses (Fig. S11). The resulting calibration curve (Fig. 6) exhibited excellent linearity, described by the regression equation $I = 0.4728\, C_{HVA} + 0.9998$, further confirming the electrode's robustness for sensitive and precise HVA detection.

3.7. Method validation

The validation outcomes for the g-C$_3$N$_4$@nZVI-modified CPE are summarized in Table 1. These results showcase the analytical method's precision, accuracy, and suitability for reliable determination of HVA in urine samples, underscoring its practical applicability as a robust diagnostic tool.

The selectivity of the sensor was evaluated by examining the electrochemical behavior of HVA in the presence of common interferents that may be excreted in urine such as ascorbic acid,

creatinine, uric acid, dopamine and glucose under the same experimental conditions. DPV responses demonstrate that the interfering species do not produce significant current responses, confirming the high selectivity of the developed sensor toward HVA detection (Fig. 7). As a result, the proposed sensor achieves high selectivity in complex urine matrices, ensuring accurate HVA quantification without extensive sample pretreatment.

To assess intra-day precision, three consecutive measurements of the anodic peak current were made using three different HVA standard solutions on the same day, and the relative standard deviation (% RSD) was calculated. For inter-day precision, identical concentration levels were measured on separate days, yielding % RSD values below 2%, demonstrating excellent reproducibility. Accuracy was verified by measuring three different HVA concentration levels and calculating recovery rates; results consistently fell within acceptable ranges, confirming the method's reliability for quantitative determinations.

3.8. Sensor stability

A long-term stability assessment of the g-C$_3$N$_4$@nZVI-modified carbon paste electrode was conducted using DPV in a standard solution of HVA. Over a 3 months period and multiple measurement sessions, the peak current remained remarkably consistent, with relative standard deviation (RSD) values well under 2%, indicating exceptional reproducibility.

Table 1 Response characterization and validation parameters obtained by the developed DPV method for determination of HVA

Parameter	Homovanillic acid
LOD (μm)	0.978
Linearity range (μM)	2.00–100.00
Slope	0.4728
Intercept	1×10^{-6}
Correlation coefficient (r)	0.9998
Accuracy (mean ± SD)	100.08 ± 1.01
Precision	
(% RSD)[a]	1.45
(% RSD)[b]	1.68

[a] Intraday precision [average of three different concentrations of three replicate each (n = 9) within the same day]. [b] Interday precision [average of three different concentrations of three replicate each (n = 9) repeated on three successive days].

Table 2 Analytical application of the developed sensor in urine samples with spiked HVA concentrations

Analytes	HVA concentration (μM)		Recovery%
	Added	Found	
HVA	10	9.5	95.00 ± 1.28
	30	29.39	97.96 ± 0.93

Table 3 Comparison of the proposed sensor performance with the reported electrochemical methods

Method/electrode	Technique	Linear range	LOD	Matrix	Key points	References
Modified Ni-doped ZnO/CPE	DPV	3.96×10^{-6} to 3.83×10^{-5} M	1.01×10^{-6} M	Urine	Good sensitivity for urinary HVA but requires very acidic conditions	2
Urea-derivative-modified graphite electrode	DPV	9.97×10^{-6} to 2.35×10^{-4} M	1.99×10^{-7} M	Buffer solutions	Limited real-sample validation	26
Modified pencil graphite electrode	DPV	3.00×10^{-6} to 6.14×10^{-5} M	1.82×10^{-6} M	Urine	Monomer concentration, polymerization cycles, and pH must be carefully optimized to achieve reproducible results	27
Poly(neutral red) (PNR/GCE)	DPV	4×10^{-6} M to 1.0×10^{-4} M	1.2×10^{-6} M	Urine	Requires very acidic conditions	28
g-C$_3$N$_4$@nZVI/CPE	DPV	2.00×10^{-6} M to 1.00×10^{-4} M	9.78×10^{-7} M	Urine	Highest sensitivity at near neutral conditions	This work

3.9. Analysis of HVA in spiked human urine

To assess method performance under realistic conditions, human urine samples were spiked with known amounts of HVA across the established calibration range of 2 to 100 μM. Published studies report typical adult urinary HVA concentrations in the range of approximately 8–41 μM,[27] placing physiological levels within the sensor's linear response window. Spiked urine specimens were diluted with PBS (pH 6.0) and analyzed *via* DPV using the g-C$_3$N$_4$@nZVI/CPE under the previously described experimental conditions. Results exhibited consistently sharp, well-defined oxidation peaks for HVA. Recoveries ranged within accepted concentration levels, demonstrating both accuracy and reliability in complex urine (Table 2). These findings confirm that the sensor performs robustly for clinically relevant HVA concentrations and is therefore suitable for point-of-care applications in real human urine samples.

3.10. Comparison of the proposed sensor with previously reported sensors

The analytical characteristics of the proposed g-C$_3$N$_4$@nZVI/CPE were compared with previously reported electrochemical methods for HVA determination, as summarized in Table 3. The present sensor exhibits a linear response between 2 and 100 μM, that fully encompasses the clinically relevant urinary HVA concentrations (8.0–41.0 μM), while operating under near-neutral pH conditions suitable for direct urine analysis. Unlike several earlier approaches that require strongly acidic electrolytes, sophisticated electrode materials, or extensive sample pretreatment, the developed platform operates under near-neutral conditions and allows straightforward analysis of diluted urine samples. While some reported sensors achieve lower limits of detection, these are often based on costly substrates or complex fabrication procedures that restrict portability and routine use. In contrast, the g-C$_3$N$_4$@nZVI/CPE combines adequate sensitivity with simple electrode preparation, good selectivity toward HVA in the presence of common urinary components, and stable performance in real matrices.

These features collectively underline the suitability of the proposed sensor for practical and decentralized HVA analysis.

4. Conclusion

Electrochemical biosensors have emerged as transformative tools in cancer diagnostics, offering rapid, sensitive, and low-cost detection of biomarkers like homovanillic acid. In this work, a hybrid nanocomposite, graphitic carbon nitride (g-C$_3$N$_4$) loaded with nanoscale zero-valent iron (nZVI), was integrated into a CPE to produce a portable sensor capable of high-performance HVA detection in urine *via* Differential Pulse Voltammetry (DPV). The modified g-C$_3$N$_4$@nZVI/CPE exhibited significantly enhanced electrochemical behavior compared to unmodified electrodes, with superior peak currents, broader linear detection range, and reduced background currents. Taken together, this work presents the first demonstration of a g-C$_3$N$_4$@nZVI-modified CPE for direct, rapid, and reliable DPV-based detection of HVA in urine. The approach aligns well with current trends in decentralized biomarker sensing and offers a practical foundation for future development of portable cancer diagnostic tools, where early, non-invasive detection can significantly enhance patient outcomes.

Ethical statement

All procedures involving human participants, including urine sample collection, were conducted in accordance with the ethical standards of the Declaration of Helsinki. Ethical approval was obtained from the Research Ethics Committee of the Faculty of Pharmacy, Cairo University, Egypt (Ethics Approval No. AC 3068). Informed consents were obtained from all participants before sample collection.

Author contributions

All authors contributed to the study conception and design. Material synthesis was performed by Amr M. Mahmoud and Aya A. Mouhamed. Data collection and analysis were performed by

Conflicts of interest

There are no conflicts of interest to declare.

Data availability

The data supporting this article have been included as part of the supplementary information (SI). Supplementary information is available. See DOI: https://doi.org/10.1039/d5ra08154h.

References

1 H. Magdelénat, Tumour markers in oncology: past, present and future, *J. Immunol. Methods*, 1992, **150**, 133–143.

2 R. Abdalla, A. M. Mahmoud, A. M. Abou Al-Alamein, M. M. Galal and D. A. El Mously, Point-of-Care Sensor Using Modified Nickel-doped Zinc Oxide Nanoparticle Carbon Paste Electrode for Homovanillic Acid Cancer Biomarker Detection in Urine, *J. Electrochem. Soc.*, 2024, **171**, 117509.

3 J. Chamberlain, Screening for neuroblastoma: a review of the evidence, *J. Med. Screen*, 1994, **1**, 169–175.

4 F. Berthold, D. H. Hunneman, D. Harms, H. Käser and J. Zieschang, Serum vanillylmandelic acid/homovanillic acid contributes to prognosis estimation in patients with localised but not with metastatic neuroblastoma, *Eur. J. Cancer*, 1992, **28**, 1950–1954.

5 E. Grouzmann and F. Lamine, Determination of catecholamines in plasma and urine, *Best Pract. Res. Clin. Endocrinol. Metabol.*, 2013, **27**, 713–723.

6 M. S. Cardoso, A. R. Rocha, J. A. Souza-Júnior and J. A. Menezes-Filho, Analytical method for urinary homovanillic acid and 5-hydroxyindoleacetic acid levels using HPLC with electrochemical detection applied to evaluate children environmentally exposed to manganese, *Biomed. Chromatogr.*, 2023, **37**, e5699.

7 V. Bhalchim, V. Undale, S. Shewale, S. Padole, P. Phadatare and A. Mali, Simultaneous detection of homovanillic acid (HVA) and vanillyl mandelic acid (VMA) in urine sample by HPLC method, *NeuroQuantology*, 2022, **20**, 1880.

8 A. Němečková-Makrlíková, J. Barek, T. Navrátil, J. Fischer, V. Vyskočil and H. Dejmková, Simultaneous determination of tumour biomarkers homovanillic acid, vanillylmandelic acid, and 5-hydroxyindole-3-acetic acid in human urine using single run HPLC with a simple wall-jet glassy carbon electrochemical detector, *J. Electroanal. Chem.*, 2020, **878**, 114629.

9 J. Mika, J. Barek, J. Zima, J. C. Moreira and H. Dejmková, Simultaneous determination of homovanillic and vanillylmandelic acid by HPLC using a coulometric detector with renewable glassy carbon microbeads based working electrode, *Electroanalysis*, 2018, **30**, 1455–1460.

10 D. Remane, S. Grunwald, H. Hoeke, A. Mueller, S. Roeder, M. von Bergen and D. K. Wissenbach, Validation of a multi-analyte HPLC-DAD method for determination of uric acid, creatinine, homovanillic acid, niacinamide, hippuric acid, indole-3-acetic acid and 2-methylhippuric acid in human urine, *J. Chromatogr. B*, 2015, **998–999**, 40–44.

11 Y. Zhou, H. Yan, Q. Xie, S. Huang, J. Liu, Z. Li, M. Ma and S. Yao, Simultaneous analysis of dopamine and homovanillic acid by high-performance liquid chromatography with wall-jet/thin-layer electrochemical detection, *Analyst*, 2013, **138**, 7246–7253.

12 M. A. Saracino, R. Mandrioli, L. Mercolini, A. Ferranti, A. Zaimovic, C. Leonardi and M. A. Raggi, Determination of homovanillic acid (HVA) in human plasma by HPLC with coulometric detection and a new SPE procedure, *J. Pharm. Biomed. Anal.*, 2006, **42**, 107–112.

13 M. Tsunoda, K. Mitsuhashi, M. Masuda and K. Imai, Simultaneous determination of 3,4-dihydroxyphenylacetic acid and homovanillic acid using high performance liquid chromatography–fluorescence detection and application to rat kidney microdialysate, *Anal. Biochem.*, 2002, **307**, 153–158.

14 A. M. Kumar, J. B. Fernandez, N. Schneiderman, K. Goodkin, C. Eisdorfer and M. Kumar, Simultaneous Determination of 5-Hydroxytryptamine, 5-Hydroxy-Tryptophan, 5-Hydroxyindoleacetic Acid, Dopamine, and Homovanillic Acid in Whole Blood, Using Isocratic Hplc With Electrochemical Detection, *J. Liq. Chromatogr. Relat. Technol.*, 1999, **22**, 2211–2223.

15 A. R. Bonfigli, G. Coppa, R. Testa, I. Testa and G. De Sio, Determination of vanillylmandelic, 5-hydroxyindoleacetic and homovanillic acid in urine by isocratic liquid chromatography, *Eur. J. Clin. Chem. Clin. Biochem.*, 1997, **35**(1), 57–61.

16 P. Van Haard, J. Wielders and J. Wikkerink, Direct concurrent measurement of urinary vanillylmandelic acid, 5-hydroxyindoleacetic acid and homovanillic acid by HPLC. Three methodologies compared, *Biomed. Chromatogr.*, 1987, **2**, 209–215.

17 J. Wielders and C. J. Mink, Analysis of vanillylmandelic acid, homovanillic acid and 5-hydroxyindoleacetic acid in human urine by high-performance liquid chromatography and fluorometry, *J. Chromatogr. Biomed. Appl.*, 1984, **310**, 379–385.

18 M. Scheinin, W.-H. Chang, K. L. Kirk and M. Linnoila, Simultaneous determination of 3-methoxy-4-hydroxyphenylglycol, 5-hydroxyindoleacetic acid, and homovanillic acid in cerebrospinal fluid with high-performance liquid chromatography using electrochemical detection, *Anal. Biochem.*, 1983, **131**, 246–253.

19 W.-H. Chang, M. Scheinin, R. S. Burns and M. Linnoila, Rapid and Simple Determination of Homovanillic Acid in Plasma Using High Performance Liquid Chromatography with Electrochemical Detection, *Acta Pharmacol. Toxicol.*, 1983, **53**, 275–279.

20 K. Sadilkova, K. Dugaw, D. Benjamin and R. M. Jack, Analysis of vanillylmandelic acid and homovanillic acid by UPLC-MS/MS in serum for diagnostic testing for neuroblastoma, *Clin. Chim. Acta*, 2013, **424**, 253–257.

21 L. Lionetto, A. M. Lostia, A. Stigliano, P. Cardelli and M. Simmaco, HPLC-mass spectrometry method for quantitative detection of neuroendocrine tumor markers: vanillylmandelic acid, homovanillic acid and 5-hydroxyindoleacetic acid, *Clin. Chim. Acta*, 2008, **398**, 53–56.

22 M. J. Magera, A. L. Stoor, J. K. Helgeson, D. Matern and P. Rinaldo, Determination of homovanillic acid in urine by stable isotope dilution and electrospray tandem mass spectrometry, *Clin. Chim. Acta*, 2001, **306**, 35–41.

23 G. Fauler, H. Leis, E. Huber, C. Schellauf, R. Kerbl, C. Urban and H. Gleispach, Determination of homovanillic acid and vanillylmandelic acid in neuroblastoma screening by stable isotope dilution GC-MS, *J. Mass Spectrom.*, 1997, **32**, 507–514.

24 R. Z. Shi, Y.-P. Ho, J. H. K. Yeung, P. M. Y. Or, K. K. W. To, M. W. M. Lau and M. Arumanayagam, Development of an enzyme-linked immunosorbent assay with monoclonal antibody for quantification of homovanillic in human urine samples, *Clin. Chem.*, 1998, **44**, 1674–1679.

25 A. Němečková-Makrlíková, T. Navrátil, J. Barek, P. Štenclová, A. Kromka and V. Vyskočil, Determination of tumour biomarkers homovanillic and vanillylmandelic acid using flow injection analysis with amperometric detection at a boron doped diamond electrode, *Anal. Chim. Acta*, 2019, **1087**, 44–50.

26 T. V. Shishkanova, F. Králík and A. Synytsya, Voltammetric detection of vanillylmandelic acid and homovanillic acid using urea-derivative-modified graphite electrode, *Sensors*, 2023, **23**, 3727.

27 S. Antherjanam, B. Saraswathyamma and S. Murugesan Senthil Kumar, Simultaneous electrochemical determination of the tumour biomarkers homovanillic acid and vanillylmandelic acid using a modified pencil graphite electrode, *Microchem. J.*, 2023, **190**, 108659.

28 S. Baluchová, J. Barek, L. I. N. Tomé, C. M. A. Brett and K. Schwarzová-Pecková, Vanillylmandelic and homovanillic acid: electroanalysis at non-modified and polymer-modified carbon-based electrodes, *J. Electroanal. Chem.*, 2018, **821**, 22–32.

29 A. Alaghmandfard and K. Ghandi, A Comprehensive Review of Graphitic Carbon Nitride (g-C_3N_4)–Metal Oxide-Based Nanocomposites: Potential for Photocatalysis and Sensing, *Nanomaterials*, 2022, **12**, 294.

30 J. Li, S. Du, Y. Wang, L. Sun, X. Fu, S. Shang, J. Liu, L. Li, G. Deng and Q. Zhang, Biodegradable silica gated poly(methylacrylate acid) core-shell microspheres for pH and glutathione dual responsive drug delivery, *J. Drug Delivery Sci. Technol.*, 2024, **100**, 106031.

31 Y. Ding, C. Deng, Y. Yang, J. Zhang, W. Liu, O. Aras, F. An, J. Liu and Y. Chai, Carrier-free nanoparticles for cancer theranostics with dual-mode magnetic resonance imaging/fluorescence imaging and combination photothermal and chemodynamic therapy, *Int. J. Pharm.*, 2025, **671**, 125285.

32 J. Li, Y. Hou, H. Wu, C. Chen, X. Fu, J. Liu, L. Li, S. Shang and G. Deng, A poly(vinyl alcohol) coated core-shell nanoparticle with a tunable surface for pH and glutathione dual-responsive drug delivery, *Colloids Surf. B Biointerfaces*, 2025, **247**, 114421.

33 J. Su, Q. Yang, Z. Zhang and Z. Zhang, Synergistic mechanisms of Ni/Fe@Fe_3O_4-g-C_3N_4 (NFFOCN) nanocomposites in efficient Cr(VI) removal from aqueous solution, *J. Water Proc. Eng.*, 2024, **68**, 106459.

34 M. A. Khan, S. Mutahir, I. Shaheen, Y. Qunhui, M. Bououdina and M. Humayun, Recent advances over the doped g-C_3N_4 in photocatalysis: a review, *Coord. Chem. Rev.*, 2025, **522**, 216227.

35 M. Liu, G. Chen, L. Xu, Z. He and Y. Ye, Environmental remediation approaches by nanoscale zero valent iron (nZVI) based on its reductivity: a review, *RSC Adv.*, 2024, **14**, 21118–21138.

36 O. Eljamal, R. Mokete, N. Matsunaga and Y. Sugihara, Chemical pathways of Nanoscale Zero-Valent Iron (NZVI) during its transformation in aqueous solutions, *J. Environ. Chem. Eng.*, 2018, **6**, 6207–6220.

37 L. Liang, F. Xi, M. Zhou and B. Hu, Efficient U(VI) removal from aerobic solution by synergistic interaction of nano zero-valent iron with g-C_3N_4 and assessment of toxicity to microorganism, *J. Water Proc. Eng.*, 2024, **64**, 105630.

38 V. Karel, Š. Ivan and R. Metelka, Carbon paste electrodes in electroanalytical chemistry, *J. Serb. Chem. Soc.*, 2009, **74**(10), 1021–1033.

39 S. S. Soliman, A. M. Mahmoud, A. A. Mouhamed and O. G. Hussein, Electrochemical sensor modified with heterostructure of graphitic carbon nitride/gold nanoparticles for non-invasive uric acid detection in saliva, *Sens. Biosens. Res.*, 2025, **50**, 100881.

40 A. A. Mouhamed, A. H. Nadim, A. M. Mahmoud, N. M. Mostafa and B. M. Eltanany, Bimetallic MOF-based electrochemical sensor for determination of paracetamol in spiked human plasma, *BMC Chem.*, 2024, **18**, 148.

41 C. Francesco, Differential Pulse Voltammetry: Evolution of an In Vivo Methodology and New Chemical Entries, A Short Review, *J. New Dev. Chem.*, 2020, **2**, 20–28.

42 B. J. Venton and D. J. DiScenza, in *Electrochemistry for Bioanalysis*, ed. B. Patel, Elsevier, 2020, pp. 27–50, DOI: 10.1016/B978-0-12-821203-5.00004-X.

43 G. Deffo, T. F. Nde Tene, L. Medonbou Dongmo, S. L. Zambou Jiokeng and R. C. Tonleu Temgoua, in *Encyclopedia of Solid-Liquid Interfaces*, ed. K. Wandelt and G. Bussetti, Elsevier, Oxford, 1st edn, 2024, pp. 409–417, DOI: 10.1016/B978-0-323-85669-0.00040-4.

44 B. M. Kanaan, H. Hendawy, O. A. Ahmed-Farid, A. M. Algohary and A. T. Soudi, A voltammetric approach for enhanced determination of Bictegravir using CB-GO based electrochemical sensor; greenness and whiteness evaluations, *Microchem. J.*, 2025, **214**, 114053.

45 S. A. Tawfik, A. M. Mahmoud and A. T. Soudi, Eco-friendly cucurbituril-based potentiometric sensors for selective quantification of ipratropium bromide in pharmaceuticals

and human plasma, *Anal. Bioanal. Chem.*, 2026, **418**, 1125–1137.

46 A. A. Mouhamed, B. M. Eltanany, N. M. Mostafa, T. A. Elwaie and A. H. Nadim, Design of screen-printed potentiometric platform for sensitive determination of mirabegron in spiked human plasma; molecular docking and transducer optimization, *RSC Adv.*, 2023, **13**, 23138–23146.

47 R. M. Tony, M. M. Galal, A. M. Mahmoud and A. T. Soudi, Application of a Solid-State Potentiometric Sensor for Point-of-care Diagnostics of Flucloxacillin in Spiked Human Plasma; Whiteness Evaluation, *Electroanalysis*, 2024, **36**, e202400069.

48 A. M. Algohary, H. Hendawy, O. A. Ahmed-Farid, B. M. Kanaan and A. T. Soudi, Breaking the chromatography barrier: a sustainable MnO$_2$-modified SPE sensor for butamirate determination in pharmaceutical and biological samples for point-of-care applications, *Microchem. J.*, 2026, **221**, 116922.

49 B. Hayes, C. Murphy, A. Crawley and R. O'Kennedy, Developments in Point-of-Care Diagnostic Technology for Cancer Detection, *Diagnostics*, 2018, **8**, 39.

50 S. A. Boltia, A. T. Soudi, E. S. Elzanfaly and H. E. Zaazaa, Development and Greenness Evaluation of a Potentiometric Method for Lomefloxacin Hydrochloride Determination in Urine and Establishment of Cumulative Excretion Pattern, *J. Electrochem. Soc.*, 2019, **166**, B141.

51 S. A. Boltia, A. T. Soudi, E. S. Elzanfaly and H. E. Zaazaa, A new plan for determining drug pharmacokinetics by establishment of urinary excretion pattern. Spectrofluorimetric application on Lomeflox® tablets, *Microchem. J.*, 2019, **148**, 419–423.

52 K. Xiao, Y. Xu, X. Cao, H. Xu and Y. Li, in *60 Years of the Loeb-Sourirajan Membrane*, ed. H.-H. Tseng, W. J. Lau, M. A. Al-Ghouti and L. An, Elsevier, 2022, pp. 499–532, DOI: 10.1016/B978-0-323-89977-2.00022-1.

53 A. A. Mouhamed, A. Elsayed, N. Mostafa, A. M. Mahmoud, A. Elshaer and A. T. Soudi, Rapid nanocatalytic approach for azo dye degradation using bi-ligand nickle based-metal organic frameworks, *BMC Chem.*, 2025, **19**, 287.

54 M. Abd Mutalib, M. A. Rahman, M. H. D. Othman, A. F. Ismail and J. Jaafar, in *Membrane Characterization*, ed. N. Hilal, A. F. Ismail, T. Matsuura and D. Oatley-Radcliffe, Elsevier, 2017, pp. 161–179, DOI: 10.1016/B978-0-444-63776-5.00009-7.

55 S. Yan, Z. Li and Z. Zou, Photodegradation Performance of g-C$_3$N$_4$ Fabricated by Directly Heating Melamine, *Langmuir*, 2009, **25**, 10397–10401.

56 P. Borman and D. Elder, in *ICH Quality Guidelines*, ed. A. Teasdale, D. Elder and R. W. Nims, 2017, pp. 127–166, DOI: 10.1002/9781118971147.ch5.

57 G. Moro, A. Silvestri, A. Ulrici, F. Conzuelo and C. Zanardi, How to optimize the analytical performance of differential pulse voltammetry: one variable at time versus design of experiments, *J. Solid State Electrochem.*, 2023, **28**, 1403–1415.

58 J. Lang, W. Wang, Y. Zhou, D. Guo, R. Shi and N. Zhou, Electrochemical Behavior and Direct Quantitative Determination of Paclitaxel, *Front. Chem.*, 2022, **10**, 834154.

59 A. J. Bard and L. R. Faulkner, *Electrochemical Methods: Fundamentals and Applications*, John Wiley & Sons, New York, USA, 2nd edn, 2012.

60 M. Zniber, P. Vahdatiyekta, S. Roy, K. Nikiforow, A. Jaiswal and T.-P. Huynh, Electrochemical detection of homovanillic acid – a breast cancer biomarker using Pluronic-modified MoS$_2$ nanosheets, *Nano Futures*, 2022, **6**, 035002.